ORIGINAL ARTICLE

Modified Algorithm Using Total Count for Calculating Myocardial Washout Rate in Single-Photon Emission Computerized Tomography

Hideyuki Miyauchi, MD, PhD[1)*], Ryohei Ono, MD[1)*], Takashi Iimori, RT[2)], Koichi Sawada, RT[2)], Keisuke Hoshi, MD[3)], Ken-ichi Hirano, MD, PhD[4)], and Yoshio Kobayashi, MD, PhD[1)]

Received: July 28, 2022/Revised manuscript received: September 8, 2022/Accepted: September 21, 2022
J-STAGE advance published: September 30, 2022

Abstract

***Background*: The arithmetic mean of washout rate (WR) (namely, AMWR) of each segment is a commonly used algorithm for calculating WR from a polar map in single-photon emission computerized tomography (SPECT). However, in this algorithm, uneven radiotracer uptake among segments affects WR calculation. To solve this possible issue, we formulated a modified algorithm for calculating WR based on the total count (namely, TCWR).**

***Methods*: The WR of iodine-123-β-methyl-p-iodophenylpentadecanoic acid (BMIPP) was calculated using TCWR and AMWR, and WR values using TCWR and AMWR were compared by disease. Participants included those without cardiovascular diseases (normal), those with CD36 deficiency, triglyceride deposit cardiomyovasculopathy (TGCV), TGCV with old myocardial infarction (OMI), and non-TGCV with OMI.**

***Results*: WR values using TCWR and AMWR did not differ significantly in the following groups: normal, 27.4 ± 8.5 and 27.3 ± 8.5% (p=0.97); CD36 deficiency, -3.2 ± 6.5 and -4.1 ± 7.4% (p=0.81); TGCV, 2.4 ± 6.3 and 2.2 ± 6.3% (p=0.93); and TGCV with OMI, -0.9 ± 7.6 and -3.7 ± 8.4% (p=0.32). However, AMWR showed a lower WR than TCWR in non-TGCV with OMI (4.8 ± 8.7 and 18.9 ± 6.7%, p=0.0008).**

***Conclusions*: TCWR is suitable for calculating WR using SPECT polar maps even in cases with heterogeneous radiotracer uptake, such as OMIs. TCWR may be applied to measuring the WR of radiopharmaceuticals other than BMIPP in investigating the pathophysiology of heart diseases.**

Keywords: CD36 deficiency, Iodine-123-β-methyl-p-iodophenylpentadecanoic acid (BMIPP), Myocardial infarction, Single-photon emission computerized tomography (SPECT), Triglyceride deposit cardiomyovasculopathy (TGCV), Washout rate

Ann Nucl Cardiol 2023; 9 (1): 19–25

Washout rate (WR) analysis of radiopharmaceuticals is utilized in nuclear cardiology to evaluate the clinical pathophysiology of the heart. Thallium-201 (^{201}Tl) is widely used as a myocardial perfusion tracer in single-photon emission computerized tomography (SPECT), and SPECT has been performed for noninvasive evaluation of coronary artery disease since the 1980s (1, 2). WR analysis using ^{201}Tl SPECT can help detect ischemic areas, particularly diffuse slow washout throughout the myocardium in multivessel disease (3, 4). Iodine-123-metaiodobenzylguanidine is an analog of norepinephrine sharing the same re-uptake pathway within the cardiac synapse, and is a target of WR analysis (5), often utilized to evaluate the sympathetic nerve activity in patients with heart failure (6). Moreover, iodine-123-β-methyl-p-iodophenylpentadecanoic acid (BMIPP) myocardial scintigraphy is used in clinical practice to assess fatty acid metabolism in

DOI: 10.17996/anc.22-00172

1) Department of Cardiovascular Medicine, Chiba University Graduate School of Medicine, Chiba, Japan
2) Department of Radiology, Chiba University Hospital, Chiba, Japan
3) Department of Pediatrics, The University of Tokyo Hospital, Tokyo, Japan
4) Laboratory of Cardiovascular Disease, Novel, Non-invasive, and Nutritional Therapeutics (CNT) and Triglyceride Research Center (TGRC), Department of Triglyceride Science, Graduate School of Medicine, Osaka University, Osaka, Japan
*These authors equally contributed to this work.

cardiomyocytes. In triglyceride deposit cardiomyovasculopathy (TGCV), a defective intracellular lipolysis results in triglyceride accumulation and energy failure. TGCV was recently registered as a novel rare cardiovascular disorder in the Orphanet, a database that provides information on rare diseases and orphan drugs (ORPHA code: 565612). Notably, a markedly decreased BMIPP WR is one of the essential criteria for TGCV diagnosis (7–9). Therefore, the accurate calculation of WR is crucial for understanding cardiovascular pathophysiology and diagnosis.

Count data for WR calculation are obtained from planar or SPECT acquisition. The SPECT WR is calculated from the count data of the polar map created by dedicated analysis software, and its calculation algorithm is similar to all software. However, in clinical practice, we sometimes encounter cases in which the pathophysiology is not consistent with the WR calculated by the software. Therefore, we aimed to propose a new WR calculation algorithm and compare it with the conventional algorithm.

Materials and methods

Selection of participants

WR could not be calculated reliably by SPECT analysis software in the myocardium, including regions with decreased BMIPP uptake in the early image. Therefore, in addition to patients without cardiovascular diseases and patients with TGCV, we included patients with specific conditions that decreased BMIPP uptake in the early image—CD36 deficiency is a human loss-of-function genetic mutation model for BMIPP uptake (10), and old myocardial infarction (OMI) may present such a clinical phenotype (11).

From January 2021 to April 2022, consecutive patients who underwent BMIPP scintigraphy were reviewed. The analysis included patients without detectable cardiovascular diseases (normal) (n=11), TGCV cases (n=14), TGCV with OMI cases (n=17), and non-TGCV with OMI cases (n=10). In addition, six cases diagnosed with CD36 deficiency between July 2014 and April 2022 were included. This study was approved by the Research Ethics Committee of Chiba University Graduate School of Medicine (HJK0050-22).

^{123}I-BMIPP SPECT

Following the protocol recommended by the Japanese Society of Nuclear Cardiology, after fasting for ≥12 h, 111 MBq of ^{123}I-BMIPP (Cardiodine; Nihon Medi-Physics Co. Ltd., Tokyo, Japan) was intravenously injected at rest. Early and delayed images were obtained after 20 and 210 min, respectively. The SPECT system used was GE Infinia Hawkeye 4 (GE Healthcare Japan, Tokyo, Japan), equipped with an extended low-energy general-purpose collimator. The collection was performed in a 64 × 64 matrix in 180° step and shoot mode with a 6° sampling angle and 60 sec/view. The pixel size and the slice width were both 5.89 mm. The energy windows for ^{123}I were 159 keV ± 10% (main) and 130 keV ± 10% (sub). Reconstruction was performed with scatter corrections using filtered back-projection (using a ramp filter) and a 10th-order Butterworth filter with 0.4 cycle/cm cutoff frequency.

SPECT analysis software

SPECT data analysis for WR calculation uses dedicated software. We used Heart Risk View-S (Nihon Medi-Physics, Co. Ltd., Tokyo, Japan), which analyzes myocardial perfusion semi-automatically, provides polar maps, and calculates the WR. This software, approved by the Ministry of Health, Labour, and Welfare of Japan, was beneficial because it could export a comma separated values (CSV) file containing the data of count and WR for each of 2400 segments (20 rows and 120 columns) of the left ventricle (LV) (12).

Definition of WR

WR is defined as the ratio of the difference between the count in the early image and the time-decay-corrected delayed image divided by the former. Three-dimensional data of the heart reconstructed from SPECT acquisition data were divided into 2400 segments with the three-dimensionally retained by using circumferential profile analysis, and representative count values in each segment were defined. This method is commonly used to create a bull's eye map, and the process was performed using Heart Risk View-S in this study. The WRs were then calculated using the sum of the representative count values for the segments in the region of interest (ROI) or the representative value in each segment, using the following formula:

$WR = [(LV\ count)_{early} - (LV\ count)_{delayed} \times v] / (LV\ count)_{early} \times 100\ (\%)$, where v is a decay correction factor calculated as $1/0.5^{(time\ interval/13.2)}$.

Conventional and new algorithms for calculating WR

A schematic diagram of the tracers in a set ROI is shown in Figure 1 and describes the two WR calculation methods used in this study. The early image (left, 8 counts) and the time-decay-corrected delayed image (right, 4 counts) are displayed. Naturally, WR would be calculated using the total tracer counts in the ROI in the early and time-decay-corrected delayed image (namely, total count WR) (Figure 1A (a)). However, SPECT analysis software commonly used in clinical practice adopts the arithmetic mean of segmental WRs as the WR of the ROI (namely, arithmetic mean WR) (Figure 1A (b)) (13). Suppose the tracers are evenly uptaken into the ROI, as in the model in Figure 1 (a), the WRs using the two algorithms would be the same 50%. In this study, we

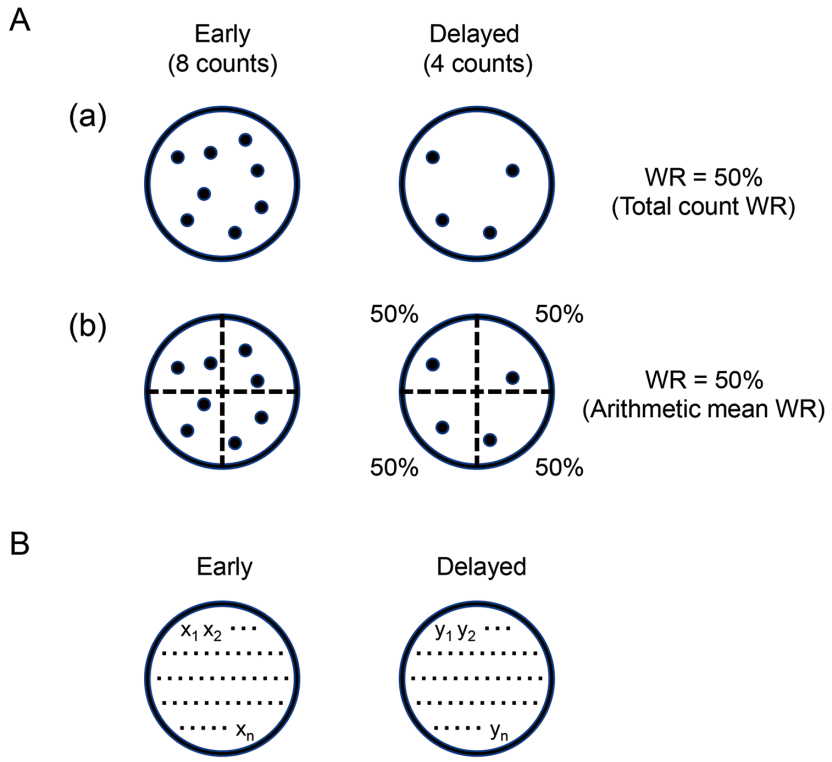

$$\text{Arithmetic mean WR (\%)} = \frac{\frac{x_1-y_1}{x_1}\times 100+\frac{x_2-y_2}{x_2}\times 100+\cdots+\frac{x_n-y_n}{x_n}\times 100}{n}=\frac{\sum_{i=1}^{n}\frac{x_i-y_i}{x_i}\times 100}{n}$$

$$\text{Total count WR (\%)} = \frac{(x_1+x_2+\cdots+x_n)-(y_1+y_2+\cdots+y_n)}{(x_1+x_2+\cdots+x_n)}\times 100 = \frac{\sum_{i=1}^{n}x_i-\sum_{i=1}^{n}y_i}{\sum_{i=1}^{n}x_i}\times 100$$

Figure 1 Calculating algorithm for WR in SPECT analysis.

A: Schematic diagram of counts in the ROIs; the early image (left, 8 counts) and the time-decay-corrected delayed image (right, 4 counts) are shown. These models represent dispersed tracers. (a) Total count WR: the algorithm of calculating WR from the total tracer counts in the ROIs in the early and delayed images. The WR is 50%. (b) Arithmetic mean WR: the conventional algorithm of calculating the arithmetic mean of WRs of each segment as the WR of the entire ROI. This diagram is divided into four segments, and the WR is 50%.

B: The definition of arithmetic mean WR and total count WR. In the early image, the ROI is divided into *n* segments, and the counts in each segment are from x_1 to x_n. Similarly, in the delayed image, the ROI is divided into *n* segments, and the time-decay-corrected counts in each segment are from y_1 to y_n.

ROI: region of interest, SPECT: single-photon emission computerized tomography, WR: washout rate

compared our formulated algorithm of total count WR with the algorithm of arithmetic mean WR.

Arithmetic mean WR

The steps for calculating the arithmetic mean WR are as follows:

1. Divide the LV into small segments and measure the counts of each segment.
2. Calculate the WR for each segment.
3. Select the WRs included in the ROI from the set of WRs.
4. Calculate their arithmetic mean.

Figure 1B shows an example of the arithmetic mean WR calculation. In the early image, the ROI is divided into *n* segments, and each count in the individual segment is defined as x_1 to x_n. Similarly, in the delayed image, the ROI is divided into *n* segments, and the time-decay-corrected count for each segment is defined as y_1 to y_n.

$$\text{Arithmetic mean WR (\%)} = \frac{\frac{x_1-y_1}{x_1}\times 100+\frac{x_2-y_2}{x_2}\times 100+\cdots+\frac{x_n-y_n}{x_n}\times 100}{n}=\frac{\sum_{i=1}^{n}\frac{x_i-y_i}{x_i}\times 100}{n}$$

Total count WR

The total count WR is the algorithm used to calculate WR from each of the total tracer counts in the ROI in the early and

time-decay-corrected delayed images (Figure 1B).

$$\text{Total count WR (\%)} = \frac{(x_1+x_2+\cdots+x_n)-(y_1+y_2+\cdots+y_n)}{(x_1+x_2+\cdots+x_n)} \times 100 = \frac{\sum_{i=1}^{n} x_i - \sum_{i=1}^{n} y_i}{\sum_{i=1}^{n} x_i} \times 100$$

Statistical analyses

We compared myocardial WR using two algorithms: total count WR and arithmetic mean WR. When a clinical indicator in the same patient is evaluated with multiple algorithms, there should not be any significant differences in the mean values between the two algorithms. If there is a significant difference, one of the algorithms may be inappropriately applied. The Bland-Altman plot may be an option for comparing their accuracies; however, the issue of accuracy evaluation does not emerge until we conclude that both algorithms are applicable. Therefore, the two algorithms were compared using Welch's t-test, assuming that the results were from different patient groups. Continuous values were reported as mean ± standard deviation. A p-value (P) <0.01 was considered statistically significant. Data were analyzed using R version 3.6.2 software (R Foundation for Statistical Computing, Vienna, Austria; https//www.R-project.org/).

Results

Figure 2 shows qualitative and quantitative comparisons of ^{123}I-BMIPP SPECT for each disease. Figure 2A displays representative polar maps of the early image (left), time-decay-corrected delayed image (middle), and the WR (right). In the normal cases, both early and delayed BMIPP uptake, and correspondingly, the WR, were normal. In CD36 deficiency, both early and delayed BMIPP uptakes were markedly decreased, and the WR was low. In TGCV patients, both early and delayed uptakes were preserved, and WR showed a characteristic decrease as a whole. In TGCV patients with OMI, defective regions of BMIPP uptake were observed in both early and delayed images, and the calculated WR was low in both defective and non-defective regions. Lastly, in non-TGCV patients with OMI, the infarcted region showed a localized decrease in WR, while the non-infarcted myocardium revealed a WR with almost no changes.

Next, we set the ROI on the whole LV and compared the total count WR with the arithmetic mean WR for each disease (Figure 2B). In the normal group, both the total count and arithmetic mean WRs were normal (27.4 ± 8.5 and 27.3 ± 8.5%, respectively, $p=0.97$). In the CD36 deficiency and TGCV patients, both the total count and arithmetic mean WRs were very low (CD36, -3.2 ± 6.5 and -4.1 ± 7.4%, p=0.81, and TGCV, 2.4 ± 6.3 and 2.2 ± 6.3%, $p=0.92$). In the TGCV patients with OMI, both the total count and arithmetic mean WRs were also very low (-0.9 ± 7.6 and -3.7 ± 8.4%, p=0.32). However, in the non-TGCV patients with OMI, while the total count WRs were within the normal range, the arithmetic mean WRs were low (18.9 ± 6.7 and 4.8 ± 8.7%, p=0.0008); this discrepancy is discussed later (please see Figure 3).

Discussion

In this study, we proposed a calculation algorithm using the total count WR as an alternative to the conventional approach with the arithmetic mean WR and compared the two algorithms. The difference between the two methods has not been emphasized so far in the literature.

Comparison of the two algorithms

Our results showed no significant differences between the two calculation algorithms for normal, CD36 deficiency, TGCV, and TGCV with OMI groups. However, a significant difference was observed in non-TGCV patients with OMI. As shown in the polar map of the non-TGCV patients with OMI (Figure 2A), the ROI includes regions with preserved and decreased WR together. Thus, in cases where uneven tracer uptake and segmental WR changes coexist, the WRs calculated using these two algorithms would be different. This finding implies that averaging the segmental WRs including outlier values has limitations in its application.

Explanatory model and future perspectives

Figure 3 shows the two models explaining possible discrepancies in WR calculation between the total count WR and arithmetic mean WR when the radiotracers are uptaken unevenly. The four different segments include five (left upper), one (right upper), one (left lower), and one (right lower) counts in the early images. In the upper model (Figure 3A), segmental counts change to 1, 1, 1, and 1 in the time-decay-corrected delayed image. In the lower model (Figure 3B), the segmental count change to 4, 0, 0, and 0 in the time-decay-corrected delayed image. Using the total count WR, because the early image and time-decay-corrected delayed image included eight and four counts, respectively, the calculated WR was 50% in both models. However, the arithmetic mean WR algorithm calculates lower or higher than the total count WR algorithm in the upper and lower models (20% or 80%, respectively). The conventional algorithm of arithmetic mean WR assumes ROIs with relatively homogeneous tracer uptake (Figure 1A) (14, 15). Mathematically, however, arithmetic mean WR sometimes exaggerates partial WR changes such as defective regions because it provides the same weight to WRs of all segments irrespective of tracer counts. Hence, when evaluating ROIs with heterogeneous tracer uptake, it is appropriate to use the whole tracer count. In addition, the total count WR is expected to

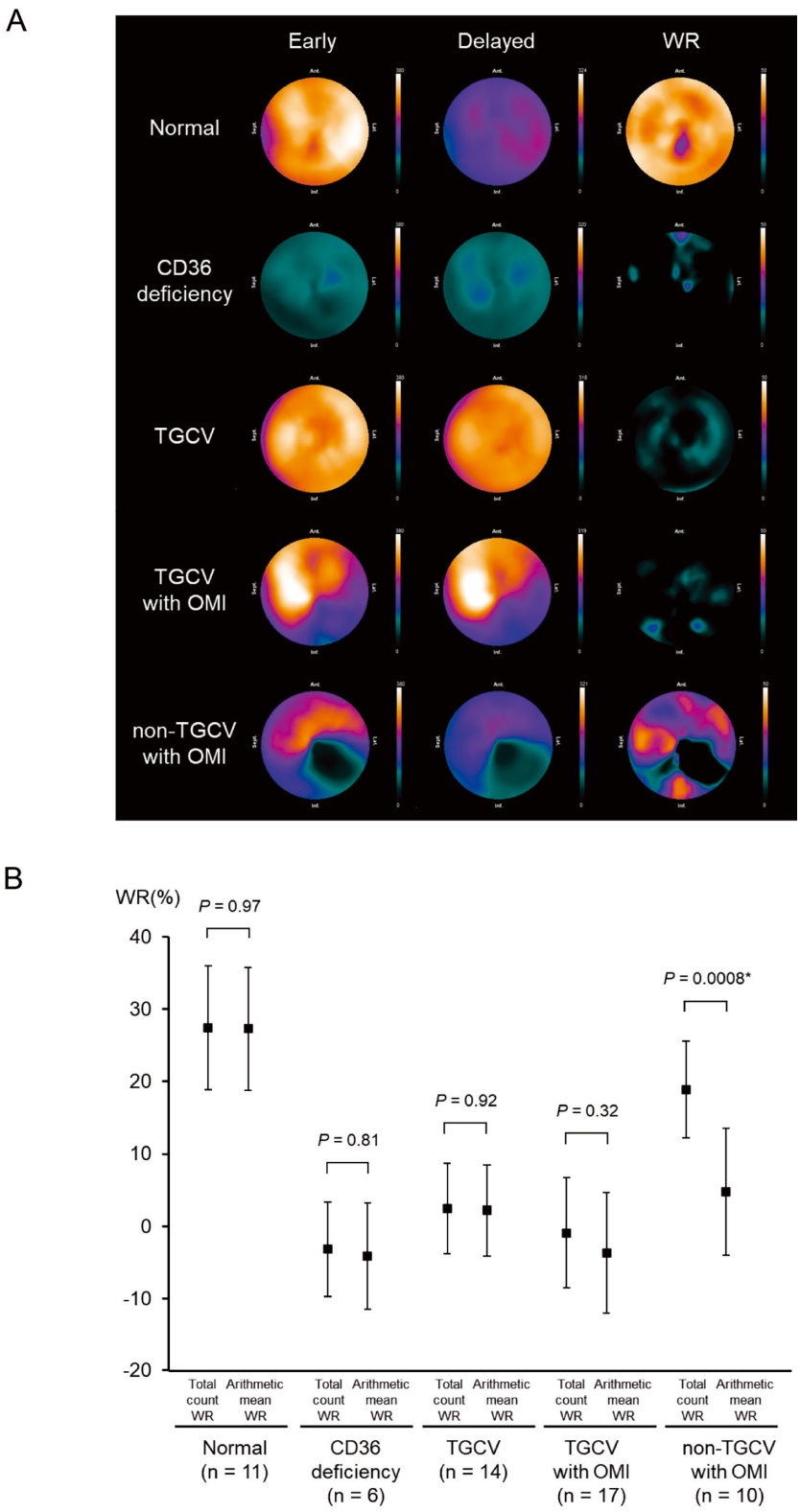

Figure 2 Qualitative and quantitative comparisons of ^{123}I-BMIPP SPECT by disease.

A: Representative ^{123}I-BMIPP SPECT polar map images: the early image (left), the time-decay-corrected delayed image (middle), and the WR (right) are shown. The color scale range of all early images is from 0 to 380 counts, the color scale of delayed images is downscaled to account for time decay correction, and the range of WR is from 0 to 50%.

B: Comparison of the total count WR and arithmetic mean WR: markers show the mean values, and bars indicate the standard deviations. ★: statistically significant

^{123}I-BMIPP: iodine-123-β-methyl-p-iodophenylpentadecanoic acid, OMI: old myocardial infarction, SPECT: single-photon emission computerized tomography, TGCV: triglyceride deposit cardiomyovasculopathy, WR: washout rate

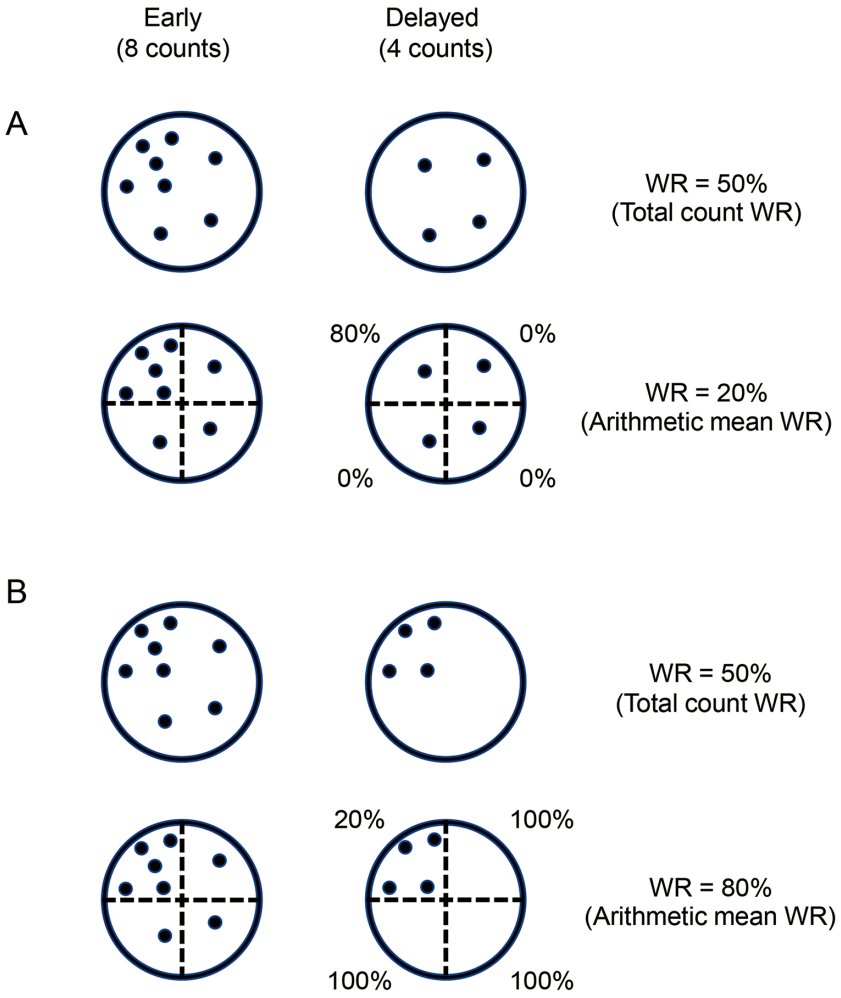

Figure 3 Two theoretical discrepancies between the total count WR and arithmetic mean WR.

Schematic diagram of counts in the ROIs: the early image (left, 8 counts) and the time-decay-corrected delayed image (right, 4 counts) are shown. These models represent tracers that are unevenly uptaken.

A: The total count WR is 50%. This diagram is divided into four segments, and the arithmetic mean WR is 20%.

B: The total count WR is 50%. This diagram is divided into four segments, and the arithmetic mean WR is 80%.

ROI: region of interest, WR: washout rate

suppress the effect of misalignment between the early and delayed images on WR. Moreover, our principle with total count WR should be valid even for local evaluation of WR and for any radiopharmaceuticals other than BMIPP. As an automatic method, we hope that the algorithm of total count WR will be equipped with SPECT analysis software in the near future.

In clinical practice for the diagnosis of TGCV

TGCV is characterized by markedly decreased BMIPP WR (9). As shown in Figure 2B, the arithmetic mean WR was remarkably decreased in non-TGCV patients with OMI, which might lead to these patients being diagnosed with TGCV. When using arithmetic mean WR, it might be confusing to differentiate TGCV which is sometimes accompanied with coronary artery disease (16), from other cardiovascular diseases with extensive myocardial necrosis. Therefore, physicians should devise a way, for example, to set an ROI in the non-defective regions.

Conclusions

In conclusion, our investigation revealed that a modified calculation algorithm using total tracer counts is a reasonable approach to calculating WR. The total count WR can be applied to interpret biological phenomena in vivo and potentially identify diseases with heterogeneous radiotracer uptake and metabolic/perfusion defects.

Acknowledgments

The authors would like to express sincere gratitude to Dr. Kenichi Nakajima, a professor at Kanazawa University, for his expertise and support in the preparation of the manuscript.

Sources of funding

None.

Conflicts of interest

The contents presented in this study are currently patent pending.

KHi and YK received grants from Nihon Medi-Physics Co. Ltd.

Reprint requests and correspondence:
Hideyuki Miyauchi, MD, PhD
Department of Cardiovascular Medicine, Chiba University Graduate School of Medicine
1-8-1 Inohana, Chuo-ku, Chiba 260-8670, Japan
E−mail: hmiyauchi@chiba-u.jp

References

1. Tamaki N, Mukai T, Ishii Y, Yonekura Y, Kambara H, Kawai C, et al. Clinical evaluation of thallium-201emission myocardial tomography using a rotating gamma camera: comparison with seven-pinhole tomography. J Nucl Med 1981; 22: 849–55.
2. Garcia EV, Van Train K, Maddahi J, Prigent F, Friedman J, Areeda J, et al. Quantification of rotational thallium-201 myocardial tomography. J Nucl Med 1985; 26: 17–26.
3. Bateman TM, Maddahi J, Gray RJ, Murphy FL, Garcia EV, Conklin CM, et al. Diffuse slow washout of myocardial thallium-201: a new scintigraphic indicator of extensive coronary artery disease. J Am Coll Cardiol 1984; 4: 55–64.
4. Koskinen M, Pöyhönen L, Seppänen S. Thallium-201 washout in coronary artery disease using SPECT—a comparison with coronary angiography. Eur J Nucl Med 1987; 12: 609–12.
5. Nakajima K, Nakata T. Cardiac ^{123}I-MIBG imaging for clinical decision making: 22-year experience in Japan. J Nucl Med 2015; 56 (Suppl 4): 11S–19S.
6. Parthenakis FI, Prassopoulos VK, Koukouraki SI, Zacharis EA, Diakakis GF, Karkavitsas NK, et al. Segmental pattern of myocardial sympathetic denervation in idiopathic dilated cardiomyopathy: relationship to regional wall motion and myocardial perfusion abnormalities. J Nucl Cardiol 2002; 9: 15–22.
7. Hirano K, Ikeda Y, Zaima N, Sakata Y, Matsumiya G. Triglyceride deposit cardiomyovasculopathy. N Engl J Med 2008; 359: 2396–8.
8. Li M, Hirano KI, Ikeda Y, Higashi M, Hashimoto C, Zhang B, et al. Triglyceride deposit cardiomyovasculopathy: a rare cardiovascular disorder. Orphanet J Rare Dis 2019; 14: 134.
9. Kobayashi K, Sakata Y, Miyauchi H, Ikeda Y, Nagasawa Y, Nakajima K, et al. The Diagnostic Criteria 2020 for triglyceride deposit cardiomyovasculopathy. Ann Nucl Cardiol 2020; 6: 99–104.
10. Hirano K, Kuwasako T, Nakagawa-Toyama Y, Janabi M, Yamashita S, Matsuzawa Y. Pathophysiology of human genetic CD36 deficiency. Trends Cardiovasc Med 2003; 13: 136–41.
11. Yoshida S, Ito M, Mitsunami K, Kinoshita M. Improved myocardial fatty acid metabolism after coronary angioplasty in chronic coronary artery disease. J Nucl Med 1998; 39: 933–8.
12. medi+FALCON® interview form (in Japanese). https://www.pmda.go.jp/PmdaSearch/kikiDetail/ResultDataSetPDF/530359_301ADBZX00045000_A_01_02
13. Chono T, Onoguchi M, Shibutani T, Hashimoto A, Nakata T, Yama N, et al. Improvement in automated quantitation of myocardial perfusion abnormality by using iterative reconstruction image in combination with resolution recovery, attenuation and scatter corrections for the detection of coronary artery disease. Ann Nucl Med 2017; 31: 181–9.
14. Omür O, Ozcan Z, Argon M, Acar ET. A comparative evaluation of Tl-201 and Tc-99m sestamibi myocardial perfusion spect imaging in diabetic patients. Int J Cardiovasc Imaging 2008; 24: 173–81.
15. Yamamoto H, Yamada T, Tamaki S, Morita T, Furukawa Y, Iwasaki Y, et al. Prediction of sudden cardiac death in patients with chronic heart failure by regional washout rate in cardiac MIBG SPECT imaging. J Nucl Cardiol 2019; 26: 109–17.
16. Miyauchi H, Iimori T, Hoshi K, Ohyama M, Hirano K, Kobayashi Y. Correlation perspectives for the diagnosis of idiopathic triglyceride deposit cardiomyovasculopathy. Ann Nucl Cardiol 2020; 6: 33–8.